

● *Original Contribution*

## ULTRASOUND DYNAMIC MICRO-ELASTOGRAPHY APPLIED TO THE VISCOELASTIC CHARACTERIZATION OF SOFT TISSUES AND ARTERIAL WALLS

CÉDRIC SCHMITT,<sup>\*†</sup> ANIS HADJ HENNI,<sup>\*</sup> and GUY CLOUTIER<sup>\*†‡</sup>

<sup>\*</sup>Laboratory of Biorheology and Medical Ultrasonics, University of Montreal Hospital Research Center (CRCHUM), Montréal, Québec, Canada; <sup>†</sup>Institute of Biomedical Engineering, University of Montreal, Montréal, Québec, Canada; and <sup>‡</sup>Department of Radiology, Radio-Oncology and Nuclear Medicine, University of Montreal, Montréal, Québec, Canada

(Received 9 December 2009; revised 2 June 2010; in final form 13 June 2010)

**Abstract**—Quantitative noninvasive methods that provide *in vivo* assessment of mechanical characterization of living tissues, organs and artery walls are of interest because information on their viscoelastic properties in the presence of disease can affect diagnosis and treatment options. This article proposes the dynamic micro-elastography (DME) method to characterize viscoelasticity of small homogeneous soft tissues, as well as the adaptation of the method for vascular applications [vascular dynamic micro-elastography (VDME)]. The technique is based on the generation of relatively high-frequency (240–1100 Hz) monochromatic or transient plane shear waves within the medium and the tracking of these waves from radio-frequency (RF) echoes acquired at 25 MHz with an ultrasound biomicroscope (Vevo 770, Visualsonics). By employing a dedicated shear wave gated strategy during signal acquisition, postprocessed RF sequences could achieve a very high frame rate (16,000 images per s). The proposed technique successfully reconstructed shear wave displacement maps at very high axial (60  $\mu\text{m}$ ) and lateral (250  $\mu\text{m}$ ) spatial resolutions for motions as low as a few  $\mu\text{m}$ . An inverse problem formulated as a least-square minimization, involving analytical simulations (for homogenous and vascular geometries) and experimental measurements were performed to retrieve storage ( $G'$ ) and loss ( $G''$ ) moduli as a function of the shearing frequency. Viscoelasticity measurements of agar-gelatin materials and of a small rat liver were proven feasible. Results on a very thin wall (3 mm thickness) mimicking artery enabled to validate the feasibility and the reliability of the vascular inverse problem formulation. Subsequently, the  $G'$  and  $G''$  of a porcine aorta showed that both parameters are strongly dependent on frequency, suggesting that the vascular wall is mechanically governed by complex viscoelastic laws. (E-mail: [guy.cloutier@umontreal.ca](mailto:guy.cloutier@umontreal.ca)) © 2010 World Federation for Ultrasound in Medicine & Biology.

**Key Words:** High-frequency ultrasound imaging, Ultrasound biomicroscopy, Dynamic micro-elastography, Viscoelasticity imaging, Animal study, Liver, Artery.

### INTRODUCTION

Certain pathologies may affect mechanical properties of living tissues. In cancer (*e.g.*, of the breast) or hepatic fibrosis, structure alterations result in a local increase in elasticity moduli. Samani *et al.* (2007) studied mechanical properties of *ex vivo* breast tumor specimens and showed that high-grade ductal carcinomas exhibited approximately 13-fold higher elasticity than either fat or fibroglandular tissues. In liver fibrosis, it has been shown that elastic moduli increased by a factor of 5.5 between

METAVIR scores 1 and 5 (Yeh *et al.* 2002). In hypertension, which precedes the development of atherosclerosis, a stiffening of the arterial wall has been documented. As an example, an increase in Young's moduli of 15% was found between hypertensive and normotensive populations (Liao *et al.* 1999). For these diseases, the development of noninvasive imaging methods that can detect such mechanical heterogeneities with adequate resolution (less than millimetric sizes) is of importance since morphology and composition of affected tissues are correlated with pathology grades.

An emerging multi-modality imaging technique is coupling high-resolution anatomic images obtained with ultrasound, with mechanical information provided by elastography. In quantitative elastography, elasticity and viscosity maps of soft tissues are assessed using dynamic

Address correspondence to: Guy Cloutier, PhD, Laboratory of Biorheology and Medical Ultrasonics, University of Montreal Hospital Research Center (CRCHUM), Montréal, Québec, Canada H2L 2W5. E-mail: [guy.cloutier@umontreal.ca](mailto:guy.cloutier@umontreal.ca)

methods based on monochromatic or transient excitation (Kruse *et al.* 2000; Tanter *et al.* 2008). The technique first implies the generation of a low-frequency (typically 50–400 Hz) harmonic or transient shear wave that propagates into the probed medium and the tracking of this wave with an ultrafast scanner that can typically produce more than 5000 images per s [either a B-mode ultrasound scanner (Sarvazyan *et al.* 1998; Sandrin *et al.* 2002; Bercoff *et al.* 2004), a Doppler ultrasound system (Taylor *et al.* 2000) or by MRI (Muthupillai *et al.* 1995)]. Because tissue elasticity (Young's modulus  $E$ ) is related to the measured shear wave velocity ( $v$ ) as  $E \cong 3 \rho v^2$ , where  $\rho$  is the assumed constant tissue density of 1100 kg/m<sup>2</sup>, this technique can quantitatively map medium stiffness. Methods were also proposed to quantify tissue viscoelasticity from the frequency dependence of shear wave velocity and by assuming a rheologic model governing the probed medium dynamic mechanical behavior (Chen *et al.* 2009; Deffieux *et al.* 2009). Nevertheless, most dynamic methods developed to date present two main limitations: a spatial resolution limited to a few millimeters due to the long wavelength of shear waves propagating within the tissue and direct estimation of mechanical information that is restricted to elastic modulus since the tissue viscous component is derived from *a priori* viscoelastic laws.

To overcome these limitations, particularly for vascular applications, numerous approaches have been proposed to calculate viscoelastic parameters. Sunagawa and Kanai (2005) extracted the viscoelasticity of carotid artery walls from acoustical velocity and attenuation measurements of shear waves (in the 0–100 Hz frequency range) generated by the blood flow and propagating from the intima to the adventitia. With dynamic elastography techniques, approaches presented by Zhang *et al.* (2005) and Woodrum *et al.* (2006) consisted in the local generation of a 100–500 Hz shear wave traveling transversally along the vessel wall and, in the study of the material elasticity as a function of frequency by tracking the wave velocity. It is important to note that each of these dynamic methods estimate only an average value of the longitudinal wall viscoelasticity along a segment of the artery at a maximum frequency typically below 500 Hz. Moreover, these studies (Sunagawa *et al.* 2005; Zhang *et al.* 2005; Woodrum *et al.* 2006) are assuming that wave characteristics are governed by the Voigt's rheologic law. It is obvious that using high-frequency shear waves, as proposed in the current study, one can study the rheologic behavior of living tissues in a range of frequencies unexplored so far and with an improved resolution.

The aim of this study was, thus, to propose a dedicated ultrasound system (ultra-high frame rate with a microscopic resolution) to track transient and harmonic shear waves generated in the 240–1100 Hz frequency

range. In addition, an inverse problem formulation, required to exploit such high spatial shear wave propagation maps, is suggested to recover tissue viscoelastic parameters (storage  $G'$  and loss  $G''$  moduli) of probed materials.

## MATERIALS AND METHODS

### *Experimental set-up and phantom design*

The experimental set-up is presented in Figure 1a. Plane shear waves were generated with a  $47 \times 85$  mm<sup>2</sup> rigid plate coupled to a mini-shaker (type 4810; Brüel & Kjær, Nærum, Denmark) and positioned on the surface of the probed phantom. Vibration signals built using Matlab (version 7.04; MathWorks, Natick, MA, USA) were transferred to the function generator (model 33250A; Agilent, Palo Alto, CA, USA) and amplified (low frequency amplifier, type 2706; Brüel & Kjær, Nærum, Denmark) before supplying the vibrator. To measure the  $y$  direction of the polarized shear wave motion, radio-frequency (RF) data were acquired with a high-frequency ultrasound probe (model RMV-710; [Visualsonics, Toronto, ON, Canada] 25 MHz, single element transducer focused at 15 mm) connected to a biomicroscope ultrasound scanner (Vevo 770; Visualsonics). To allow frame rates higher than 1 kHz, as obtained in ECG-gated kilohertz visualization (EKV) mode with this scanner (Chérin *et al.* 2006) and to limit motion artifacts during shear-wave gated (SW-gated) synchronization, the mono element transducer was held fixed (no oscillation back and forth). Thus, the transducer casing was automatically moved to scan the phantom along the  $x$  axis with a positioning step motor. An electronic circuit (SYNC) was designed for SW-gated synchronization to reconstruct in postprocessing RF sequences at a high frame rate of 16,000 images per s (see details below). The analog RF-output of the scanner was digitized at 500 MHz with an acquisition card (model 8500 CS; Gagescope, Montreal, QC, Canada).

For the dynamic micro-elastography (DME) study, characterizations were conducted on two large homogeneous cubic samples ( $50 \times 50 \times 50$  mm<sup>3</sup>) of agar (3%) and gelatin (3%) and on a small irregular fresh healthy rat liver ( $\approx 25 \times 15 \times 5$  mm<sup>3</sup>). To facilitate the propagation of shear waves and coupling with the oscillating plate, samples were embedded in a homogenous agar (3%) (number A-6924; Sigma Chemical, Saint-Louis, MO, USA) and gelatin (4%) (number G-2500 type A from porcine skin; Sigma Chemical) parallelepipedic phantom ( $85 \times 85 \times 95$  mm<sup>3</sup>) having a known storage modulus of 14,600 Pa (Hadj Henni *et al.* 2008), which may mimic body mechanical structures surrounding the organ of interest.

For vascular dynamic micro-elastography (VDME), phantoms mimicking vascular geometries were of two

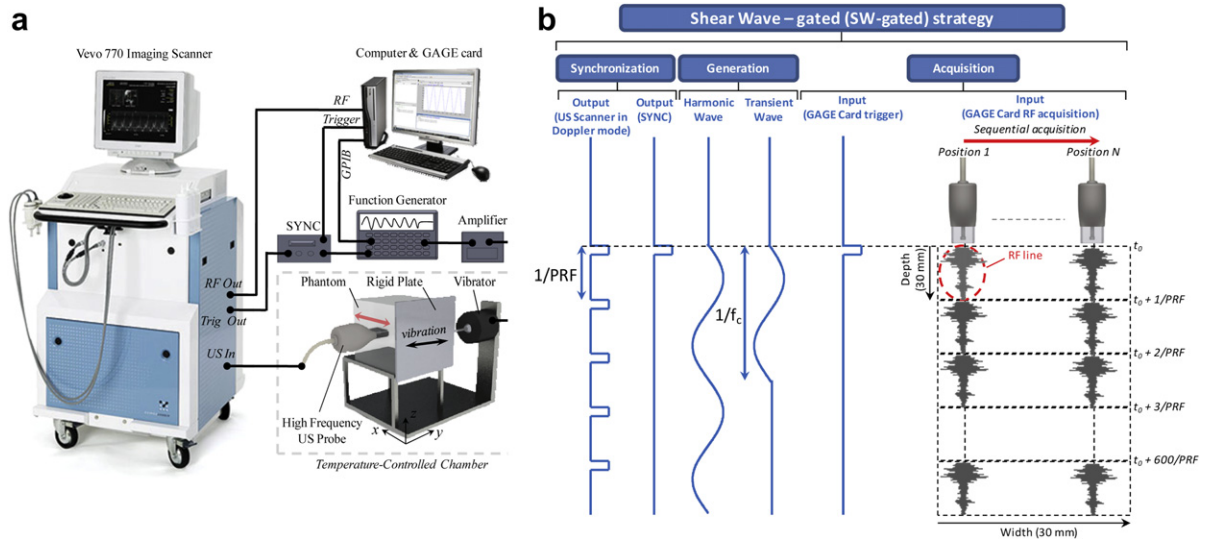


Fig. 1. *In vitro* experimental set-up used to generate and track shear waves to perform dynamic micro-elastography (a). Shear wave-gated strategy implemented to reconstruct high frame rate RF sequences (b). Ultrasound scanner in Doppler mode (at a desired pulse repetitive frequency, PRF) connected to a dedicated electronic circuit (SYNC) is used to synchronize the generation of shear waves (harmonic or transient waves at the central frequency  $f_c$ ).

types: a mimicking carotid artery made of agar (3%) and gelatin (20%) and an explanted healthy porcine abdominal aorta. These unpressurized vessels were oriented vertically in the  $z$  direction and embedded in a homogenous gel of 14,600 Pa, as done for the other phantoms. Their lumens were filled with degassed water. The lumen diameter (8 mm), wall thickness (3 mm) and length (80 mm) mimicked a human common carotid artery, whereas porcine aorta dimensions were, respectively, 13 mm, 2.8 mm and 80 mm. The animal specimen was placed in Krebs solution immediately after excision and tested within 5 h.

*RF data acquisition and post-processing*

The acquisition protocol consisted in generating harmonic (20 oscillations) and transient (six oscillations modulated with a Blackman temporal window) plane shear waves, ranging from 240–1100 Hz with 200 Hz or 50 Hz steps, respectively. The retrospective strategy used to reconstruct RF sequences at a high frame rate is schematized in Figure 1b. The Doppler mode was selected and configured with a pulse repetitive frequency (PRF) of 16 kHz. This high PRF was necessary to track vibrations with at least 10 samples per period. During a typical experiment, the transducer was moved at 120 different  $x$  positions along a distance of 30 mm. When firing at position  $N$ , a low frequency vibration was synchronized and generated within the medium. Then, 600 consecutive RF lines were acquired at a 30 mm depth. This process was sequentially repeated for each transducer position. The off-line retrospective postprocessing consisted in reassembling

collected data to reconstruct the matrix width  $\times$  depth  $\times$  time (30 mm  $\times$  30 mm  $\times$  37.5 ms). Successive ultrasonic signal propagation paths over time served as input for a one-dimensional (1-D) cross-correlation technique that was used to accurately compute motions due to shear wave propagation within the medium.

*Formulation of forward and inverse problems*

*Homogeneous agar-gelatin and liver media.* In the first model, we considered theinsonified medium as homogeneous, isotropic, linear-viscoelastic and incompressible. The complex stationary displacement field induced by the propagation of a harmonic plane shear wave propagating following the  $x$  direction and polarized in the  $y$  direction is described by,

$$U_y^H(x) = U_0 e^{i(k' + i\alpha)x} e^{i\phi} \tag{1}$$

where,  $U_0$  denotes the absolute wave amplitude and  $\phi$  is an arbitrary phase. Parameters  $k'$  and  $\alpha$  represent the real and imaginary (attenuation) parts of the wavenumber  $k$ , respectively. The subscript  $H$  indicates the homogeneous medium. Note that eqn (1) also applies for a transient excitation, when a given harmonic is considered.

The wave velocity  $v$  was calculated from the wavenumber real part  $k'$ , and the shear wave frequency  $f_{wave}$ , as:

$$v = \frac{2\pi \times f_{wave}}{k'} \tag{2}$$

The inverse problem leading to the estimate of the attenuation  $\alpha$  was evaluated as the slope of the linear

regression applied on the natural logarithm of the absolute part of  $U_y^H(x)$  (Catheline *et al.* 2004), as given below:

$$\alpha = \arg \min_{\alpha} \|\ln[\text{abs}(U_y^H(x))] - (\alpha x + b)\|_2^2. \quad (3)$$

Without any assumption on the viscoelastic model of the experimental data, the complex shear modulus defined as  $G(\omega) = G'(\omega) + iG''(\omega)$  and the wavenumber  $k = k' + i\alpha$  are related through the shear wave propagation equation as:

$$G(\omega) = \rho \frac{(2\pi \times f_{\text{wave}})^2}{k^2} \quad (4)$$

Moreover, as proposed by Vappou *et al.* (2009), the real and imaginary parts of eqn (4) can be rewritten as:

$$G'(\omega) = \rho \omega^2 \frac{k'^2 - \alpha^2}{(k'^2 + \alpha^2)^2} \quad (5)$$

$$G''(\omega) = -2\rho \omega^2 \frac{k'\alpha}{(k'^2 + \alpha^2)^2} \quad (6)$$

Using eqns (5) and (6), the storage modulus  $G'(\omega)$ , measuring the stored energy (elastic behavior) and the loss modulus  $G''(\omega)$ , representing the dissipated energy (viscous behavior), were calculated from the estimated wave velocity and attenuation.

In practical terms, after calculation of the spatio-temporal displacement fields induced by shear waves with the motion estimator, spectral analysis was used to calculate the complex stationary displacement field  $U_y^H(x,y,\omega)$  for each excitation frequency. The wave velocity was retrieved in two steps: a spatial Fourier transform was first applied to the real part of the stationary displacement fields to obtain  $k'$ , which then resulted by the mean of eqn (2), in the shear wave velocity  $v$ . The wave attenuation was calculated by minimizing the cost function of eqn (3). In harmonic mode, the spectral analysis was processed at the generated vibration frequency. In transient mode, by taking into account the wideband nature of the transmitted spectrum, the acoustical information used to characterize each medium was limited to a 200 Hz spectral window (with a frequency step of 1 Hz) centered at the applied vibration frequency. This spectral bandwidth was selected to ensure that stationary displacement maps, used in the inverse problem formulation, presented high signal-to-noise ratios. The analysis of transient spectra had the advantage of providing continuous  $G'(\omega)$  and  $G''(\omega)$  evolutions over a large frequency range and with a fine discretization.

*Vascular agar-gelatin and aortic geometries.* For vascular applications, we considered a two-dimensional (2-D) analytical model developed by Hadj Henni *et al.*

(2007) to simulate the diffraction of a harmonic or transient plane shear wave by a hollow cylinder embedded in a different medium. Both media were assumed to be homogeneous, isotropic and linear viscoelastic in the frequency domain  $G_k = G'_k + iG''_k$ , where  $k = 1$  and  $2$  indicates the cylindrical vascular inclusion and the surrounding medium, respectively. The cylinder inner surface was assumed to be unpressurized, *i.e.*, with no stress at the boundary (as performed experimentally). The displacement field, which was entirely contained in the propagation plane ( $oxy$ ) of the incident shear wave, since no displacement occurred following the  $z$  axis, satisfied the Navier differential equation.

By writing this equation in the frequency domain and in a cylindrical system of coordinates, the Helmholtz decomposition into potentials could be applied to the displacement field in each medium of the phantom. This decomposition allowed, after some developments, to express the displacement field as infinite series of Bessel and trigonometric functions containing unknown weighting coefficients. Following Hadj Henni *et al.* (2007), by taking into account the appropriate boundary conditions, expressed in terms of displacements and stress, and by formulating the solution using a transfer matrix formulation, we obtained the stationary searched theoretical displacement fields  $U_y^S(x,y,\omega)$  at the frequency  $\omega$ . The subscript  $S$  here indicates the simulated wave equation in the surrounding medium and embedded vascular geometry.

This theoretical model served to formulate an inverse problem (IP) to recover the viscoelasticity of vessel walls. The IP schematic overview is presented in Figure 2. After calculating shear wave motions  $U_y(x,y,t)$  from RF sequences  $I_{RF}(x,y,t)$ , the spectral analysis (Fourier transform) enabled the extraction of the experimental real part of the complex stationary shear wave amplitude  $\text{Re}[U_y^E(x,y,\omega)]$  at the explored frequency. The subscript  $E$  refers to experimental measures. The next step was to calculate the surrounding medium storage ( $G'_2$ ) and loss ( $G''_2$ ) moduli with the method described in the previous section for a homogenous region of interest located 10 mm above the lumen center, which was far enough from the vessel to avoid the effect of diffracted waves. The vessel wall parameters ( $G'_1, G''_1$ ) were assessed by minimizing the least mean square error between normalized simulations [which supplied the theoretical stationary map  $U_y^{S(i)}(x,y,\omega)$  at the iteration  $i$ ] and the experimental data  $U_y^E(x,y,\omega)$ . The initial conditions ( $G'_{1_0}$  and  $G''_{1_0}$ ) were arbitrarily chosen according to an *a priori* medium knowledge, then a bounded nonlinear least-square problem solver (Matlab 7.04) iterated until stopping criteria were reached.

These criteria were defined by the maximum number of iterations allowed (typically below 40) or when the

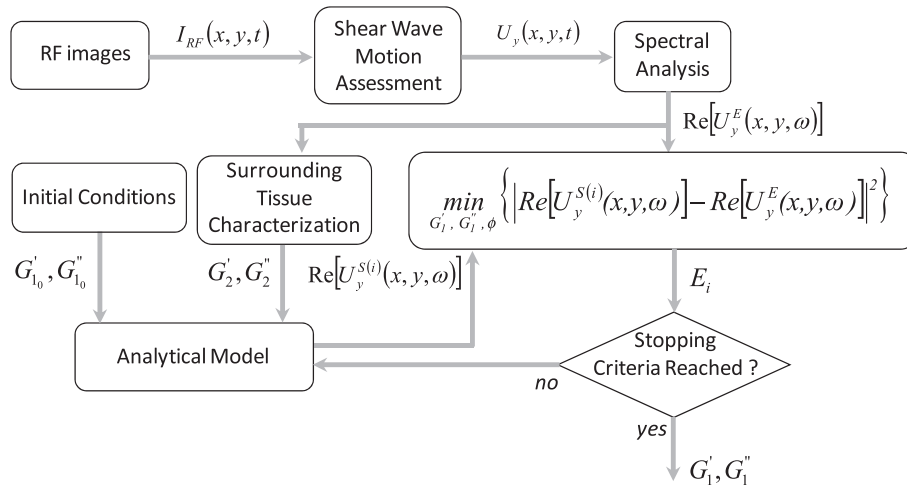


Fig. 2. Block diagram of the inverse problem used to estimate, from radio-frequency (RF) images, the complex modulus  $G$  of the vessel wall.

change of vector parameters ( $G'$ ,  $G''$ ,  $\phi$ ) or the cost function during a step became inferior to  $10^{-10}$ . Information used in the cost function was built from three RF lines within each phantom: one along the  $x$  direction centered in the middle of the wall and two positioned at  $y \pm 1/4$  of the wall thickness. For any position on these selected lines, the material was mainly subjected to shearing following the  $y$  direction, which corresponds to the radial direction according to the wall geometry. The proposed inverse problem formulation thus characterized radial moduli.

## RESULTS

### DME of homogeneous agar-gelatin and liver materials

*Parallelepipedic agar-gelatin samples.* We first investigated the evolution of  $G'$  and  $G''$  as a function of the vibration frequency in the tested materials. Typical 2-D stationary shear wave displacement maps, corresponding to an excitation frequency of 500 Hz, are presented in Figure 3 for samples 1 (Fig. 3a) and 2 (Fig. 3b), whereas 1-D profiles following the  $x$ -axis are plotted in Figure 3c. Experimental results on two samples are plotted in Figure 3d for  $G'$  and  $G''$  as a function of frequency for harmonic and transient waves.  $G'$  and  $G''$  represent the mean ( $M$ ) estimation for a depth between 10 mm to 18 mm within the block of gel; the standard deviations ( $STD$ ) are not displayed because the coefficients of variation were negligible ( $STD/M < 1\%$ ). Storage moduli ( $G'$ ) of gels in harmonic and transient modes were quasi-independent of frequency whereas loss moduli ( $G''$ ) slightly increased over the explored frequency band. The following assessment confirms the similarity of results for both excitation modes, particularly for  $G'$ . Indeed, when we compute for both storage and loss

moduli the average over frequency of the percent difference coefficient  $\text{Diff}_{H-T}$ , defined as the absolute modulus difference in harmonic ( $H$ ) and transient ( $T$ ) modes divided by the average modulus of the same two values, we obtained  $\text{Diff}_{H-T} = 8.0 (\pm 1.8) \%$  for  $G'$  and  $37.2 (\pm 27.5) \%$  for  $G''$  with sample 1, and  $\text{Diff}_{H-T} = 2.8 (\pm 1.3) \%$  for  $G'$  and  $20.9 (\pm 13.4) \%$  for  $G''$  with sample 2.

*Rat liver sample.* The second experiment was undertaken on a healthy rat liver. A B-mode image of the phantom is presented in Figure 4a with a manual segmentation of the gel-liver boundary. Figure 4b shows the real stationary displacement field ( $\text{Re}[U_y^H(x, y, \omega)]$ ) for a transient excitation frequency of 600 Hz. The liver geometry induced a change in shear wave propagation orientation ( $\vec{\psi}$  direction) at the interface of the two materials (Fig. 4b).  $G'$  and  $G''$  extracted from transient waves (Fig. 4c) were estimated within a  $1.75 \times 8 \text{ mm}^2$  region-of-interest (region B on Fig. 4b) along 20 RF lines orthogonal to the shear wave orientation  $\vec{\psi}$ . Mean and standard deviation values were calculated by studying variability of parameters following the  $\vec{\xi}$  direction (orthogonal to the  $\vec{\psi}$  direction) in the frequency range of 250–630 Hz (Fig. 4c). As observed, changes in frequency had few impacts on the storage modulus ( $G' = 1192.4 \pm 61.6 \text{ Pa}$ ), whereas  $G''$ , which denotes the dissipation of energy by the material, strongly increased as the frequency rose ( $G'' = 96.7 \pm 7.9 \text{ Pa}$  at 250 Hz vs.  $409.0 \pm 116.5 \text{ Pa}$  at 630 Hz).

### VDME of agar-gelatin and aortic samples

*Vascular agar-gelatin sample.* VDME was first applied on a mimicking artery to investigate the possibility of experimentally generating and measuring 540 to 670 Hz transient plane shear waves within a thin

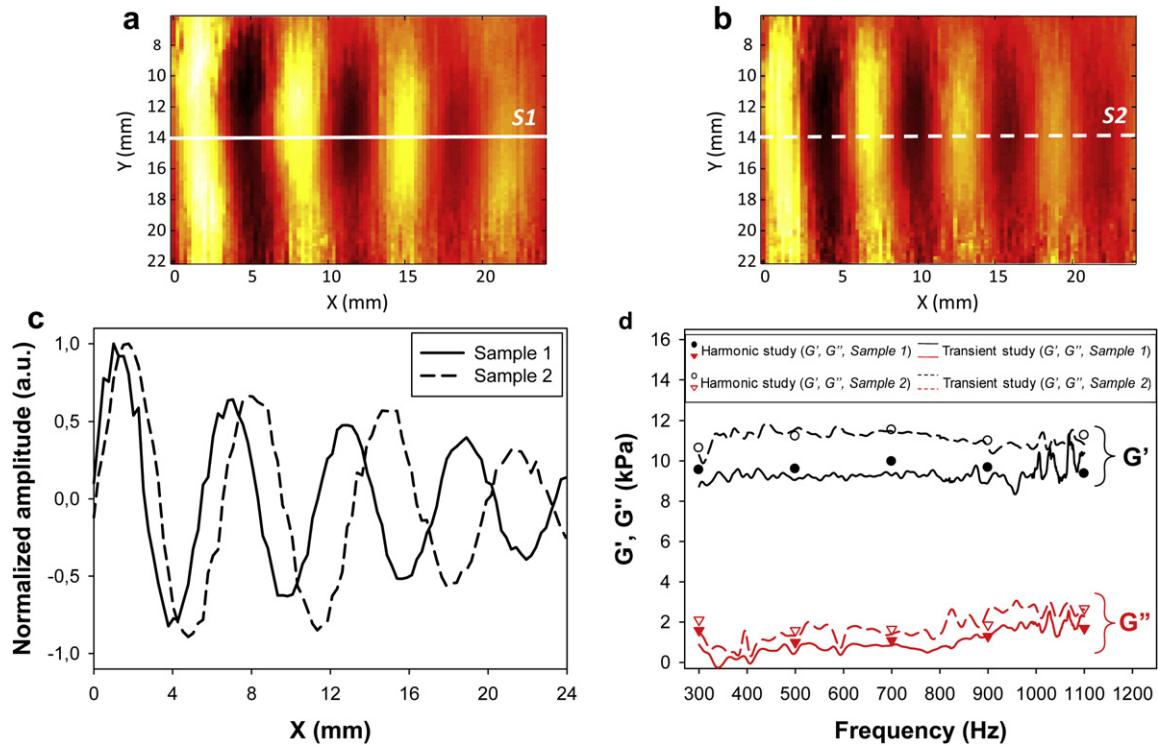


Fig. 3. Two-dimensional (2-D) stationary shear wave displacement maps at an excitation frequency of 500 Hz in gel phantoms [sample 1 in panel (a), sample 2 in panel (b)] and corresponding profiles on lines S1 [panel (a)] and S2 [panel (b)] in (c). Experimental storage ( $G'$ ) and loss ( $G''$ ) moduli for agar-gelatin samples calculated for monochromatic (symbols) and transient (line graphs) shear wave propagation (d).

wall. This experiment also served to validate the inverse problem coupled to the analytical theoretical model for viscoelasticity recovering. Figure 5 presents a typical propagation of a 550 Hz transient shear wave into the investigated vascular phantom at different moments. The shearing source, positioned at  $x = -15.0$  mm, generated a plane shear wave which, during its propagation through the phantom, was diffracted by the thin-wall agar-gelatin cylinder. The resulting refracted wave presented a circular pattern (Fig. 5b-e); *i.e.*, that the wave propagated along the wall curvature. Local transient motions within the surrounding embedding gel and vascular wall are plotted in Figure 5g for the position A displayed in panel f ( $y = 0.0$  mm,  $x = -13.5$  mm) and in Figure 5h for position B ( $y = 0.0$  mm,  $x = -4.25$  mm). The wave motion was misestimated for deeper regions ( $y > 8.0$  mm) because of low signal-to-noise ratio at such depths (high acoustical attenuation).

Taking into account the wideband nature of transient wave spectra, the acoustical information used to characterize the vascular medium was contained in a 200 Hz spectral window centered at the applied vibration frequency with a frequency step of 10 Hz. Applying such signal processing for many transient excitations allowed to assess  $G'$  and  $G''$  between 540 Hz and 670 Hz,

with a spectral discretization of 10 Hz. The experimental 550 Hz normalized stationary shear wave displacement map (Fig. 6a) corroborated the simulation following IP convergence (Fig. 6b). Experimental (line B on Fig. 6a) and simulated (line C on Fig. 6b) displacement profiles are plotted on Figure 6c for quantitative comparison ( $y = -5.5$  mm,  $-15$  mm  $< x < 15$  mm). Wave traveling in the surrounding tissue ( $-15$  mm  $< x < -4.5$  mm) clearly exhibited shorter wavelengths than in the wall ( $-4.5$  mm  $< x < 4.5$  mm).

$G'$  and  $G''$  assessed by the proposed IP at different frequencies are plotted in Figure 6d (vascular phantom data). The method retrieved  $G'$  and  $G''$  and shows values quasi independent of the frequency within 540–670 Hz ( $G = 45.4 (\pm 2.3) + i3.2 (\pm 0.5)$  kPa).

*Porcine aorta.* VDME was also applied to the mechanical characterization of a fresh healthy porcine abdominal aorta at frequencies ranging from 240 Hz to 480 Hz. As observed earlier for the mimicking artery, similar patterns of refraction were present along the wall (Fig. 7b), except that the wave within the thin aortic wall traveled slower than into the surrounding tissue at low-shear wave frequencies. This visual observation (videos not shown) is confirmed by the estimated values

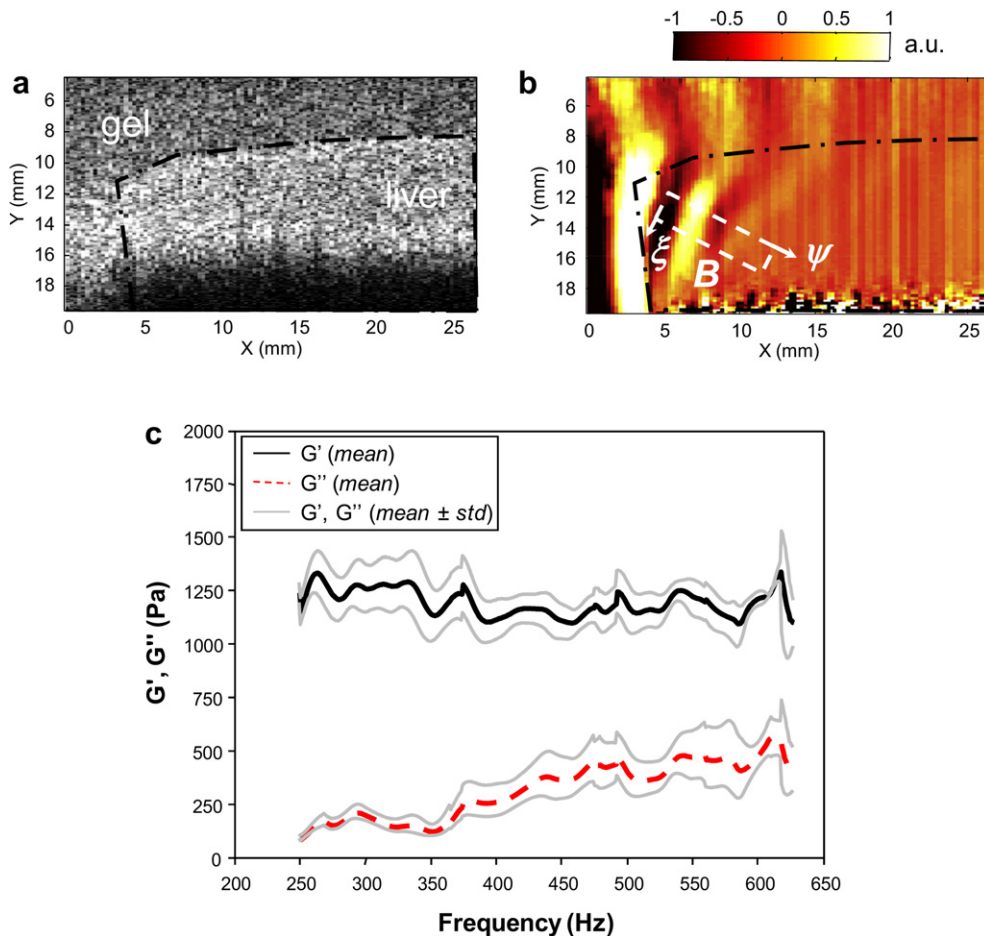


Fig. 4. B-mode image of a probed phantom made of a rat liver (region defined by the dot-dashed line) embedded in an agar-gelatin gel (a). Normalized two-dimensional (2-D) stationary shear wave displacement maps for the corresponding phantom at an excitation frequency of 600 Hz (b). Experimental mean storage (black solid line) and loss (red dot line) moduli calculated for the region of interest  $B$  (dot-dashed line) on the panel (b) with corresponding standard deviations (solid gray lines) (c).

of  $G'$  and  $G''$  (Fig. 6d, fresh porcine aortic data), which exhibit strong viscoelastic and dispersion effects.  $G'$  spreads from 5 kPa at 240 Hz to 17.5 kPa at 480 Hz, whereas  $G''$  increases from 232 Pa to 1010 Pa over the same range of frequency.

## DISCUSSION

The main purpose of this study was to evaluate the capability of DME to characterize viscoelasticity of mimicking and fresh living tissues with homogenous (agar-gelatin block and rat liver) and vascular (mimicking vessel and pig aorta) geometries in the micrometric scale over a wide range of excitation frequency. Such mechanical information may prove to be of value for small-animal imaging and clinical diagnosis. Contrary to conventional dynamic elastography methods applied to image large regions with a millimetric spatial resolution [*e.g.*, breast (Tanter et al. 2008) and brain (Kruse et al. 2008)], the

proposed technique allowed to obtain a spatial resolution of  $\approx 60 \mu\text{m}$  axially and  $250 \mu\text{m}$  laterally, and a very high temporal resolution (PRF = 16 kHz). Indeed, a very high axial resolution could be reached by the use of a high-frequency ultrasound biomicroscope working at 25 MHz central frequency [reported axial resolution of  $61.6 \mu\text{m}$  (Zhou et al. 2002), compared with around  $220 \mu\text{m}$  in resolution for 7 MHz probes]. By moving laterally the ultrasound probe at 120 positions over a 30 mm width, the lateral resolution could be that of the focused beam [*i.e.*,  $\approx 250 \mu\text{m}$  (Zhou et al. 2002)].

### Shear-wave gated strategy

Shearing tissues with relatively high-frequency waves (240–1100 Hz) ensured small wavelengths (as short as 1.7 mm in the  $x$  direction for the rat liver experiment at the maximum scanned frequency of 630 Hz), thus, improving viscoelasticity characterization. The temporal

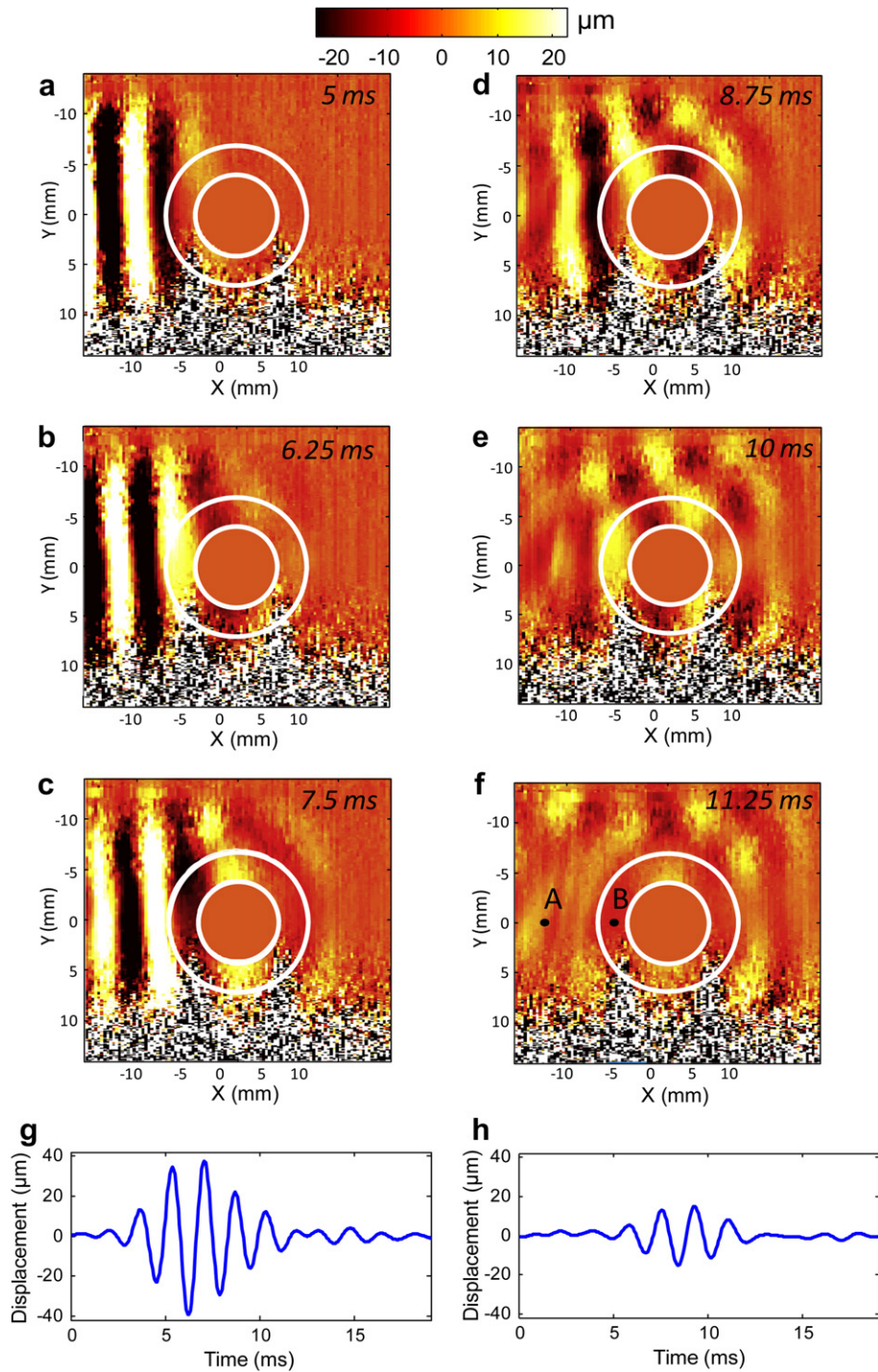


Fig. 5. Typical two-dimensional (2-D) displacement maps as a function of time of a 550 Hz transient shear wave for a mimicking artery phantom made of agar-gelatin (a-f), and associated displacement profile at positions A and B on panel (f), in (g) and (h), respectively.

resolution of  $62.5 \mu\text{s}$  (PRF = 16 kHz) was critical to ensure a fine discretization of the wave propagation (at least 10 samples per wave period, even at the highest frequency of 1100 Hz used for the agar-gelatin block experiments). Since the PRF of the high-frequency

Visualsonics scanner in Doppler mode can be adjusted to any values as high as 96 kHz, the reconstructed SW-gated RF sequences could have been selected at a higher frame rate in this study. Note that displacements induced within probed tissues were found to be very small

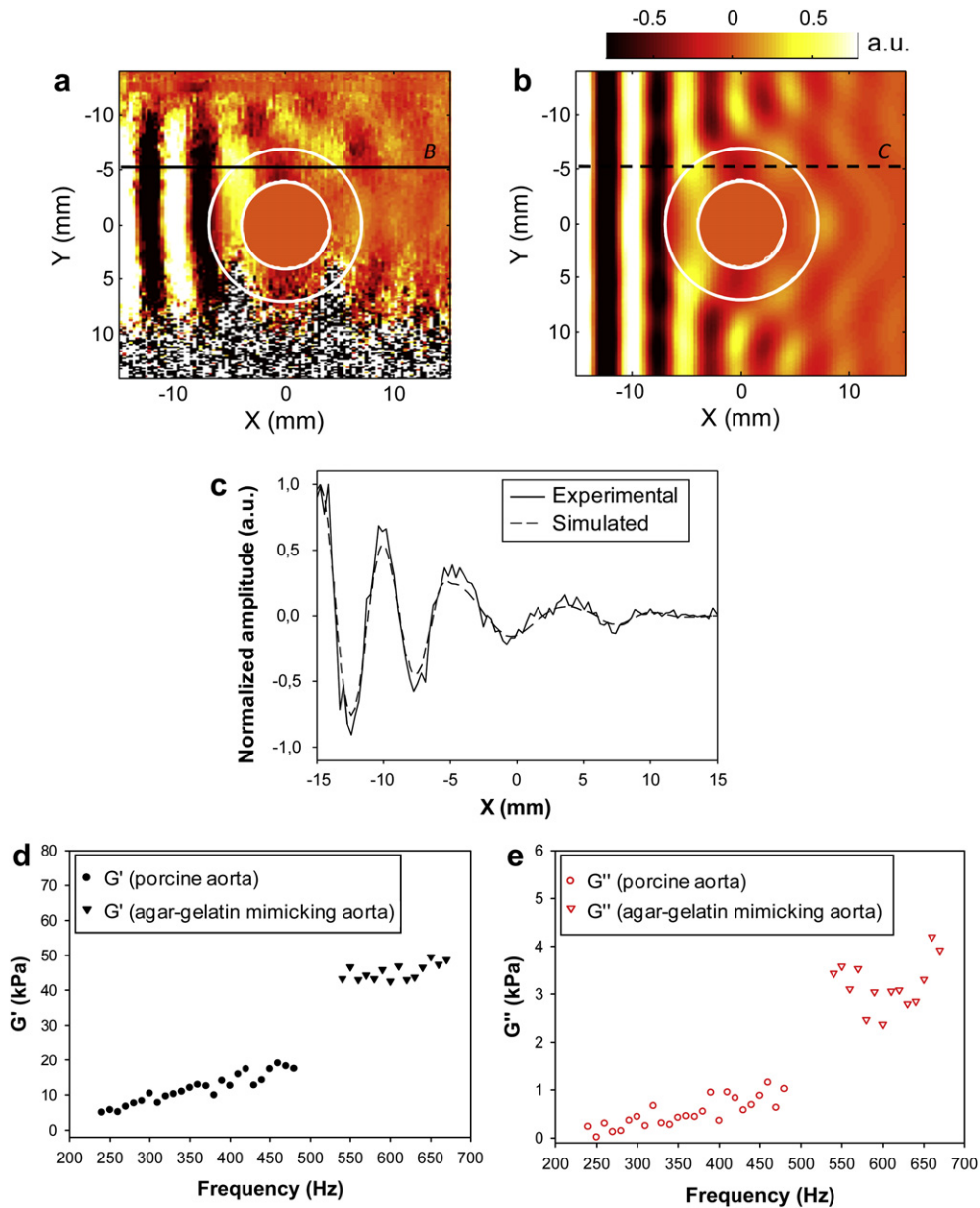


Fig. 6. Experimental (a) and simulated (b) 550 Hz two-dimensional (2-D) normalized stationary displacement maps and corresponding profiles on lines B [panel (a)] and C [panel (b)] in (c).  $G'$  (d) and  $G''$  (e) evolution as a function of frequency calculated by the VDME method on the mimicking vascular phantom (circles) and on a fresh porcine aorta (triangles).

(typically  $\pm 40 \mu\text{m}$  in the homogenous agar-gelatin materials and  $\pm 15 \mu\text{m}$  in the mimicking artery and porcine aorta) with a resolution as low as  $1 \mu\text{m}$ .

#### Literature on dynamic micro-elastography (DME)

According to the literature, displacement maps in the microscopic range were only reported with magnetic resonance elastography (Othman et al. 2005). High-frequency shear waves served to characterize brain (by mechanical tests (Nicolle et al. 2005)) and cartilage tissues [by MRI (Lopez et al. 2008)], but, as per current knowledge, no

studies have been dedicated to livers at those frequencies. The harmonic and transient comparison allowed to conclude that the easiest and fastest mode to implement (*i.e.*, transient excitation) is appropriate to study viscoelasticity of soft materials. The  $G'$  and  $G''$  parameters presented in this article were retrieved from a single data set (single shear wave propagation) without any averaging. The estimations, in both transient and harmonic modes, could thus have been considerably improved by averaging complex stationary displacement fields calculated from multiple shear wave propagations. As also

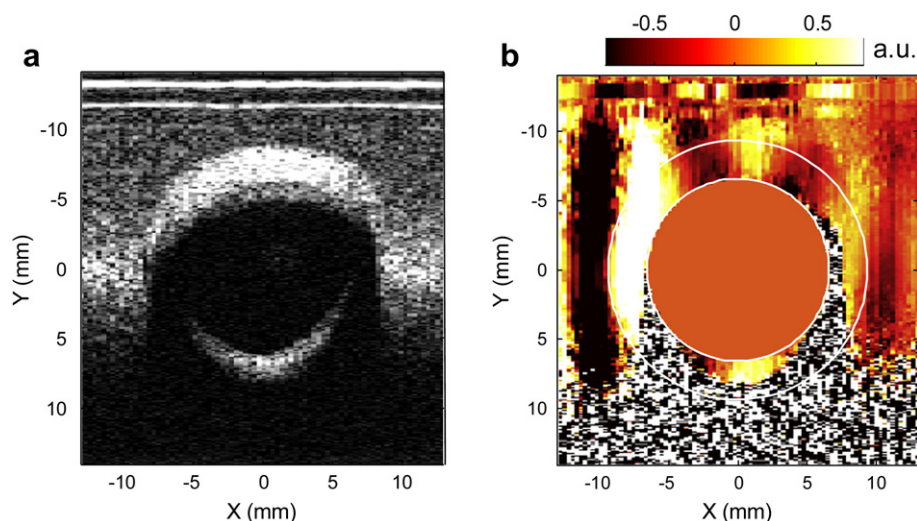


Fig. 7. B-mode image of a probed phantom made of a porcine aorta embedded in an agar-gelatin gel (a). Normalized two-dimensional (2-D) stationary shear wave displacement maps for the corresponding phantom at an excitation frequency of 350 Hz (b).

noted, the transient excitation has the advantage of furnishing fine discretization of complex modulus estimation, allowing a more robust rheologic model fitting. Quantitatively, estimated storage moduli in rat livers were in agreement with previous works for equivalent frequencies [ $G' = 1.46 \pm 0.37$  kPa at 200 Hz in Salameh *et al.* (2007),  $G' = 1.82 \pm 0.22$  kPa at 300 Hz in Salameh *et al.* (2009),  $G' = 1.38 \pm 0.20$  kPa at 120 Hz in Yin *et al.* (2007) and  $G' = 1.50 \pm 0.10$  kPa for acoustical radiation force impulse excitation (ARFI) in Wang *et al.* (2009)].

#### Literature on vascular dynamic micro-elastography (VDME)

Because of the resolution of the ultrasound scanner, the proposed approach was able to generate and track 240–670 Hz plane shear waves and measure the wave displacement field within a wall as thin as 2.8 mm. The IP formulation, accompanied by an analytical model simulating the diffraction of plane shear waves by a vessel, was validated by experiments with mimicking vascular phantoms containing either a gel or a real artery. Contrary to other noninvasive dynamic techniques, which only study  $G'$  of the wall (Woodrum *et al.* 2006) or retrieve  $G''$  by studying the frequency dependence of wave velocity coupled to a known viscoelastic model (Zhang *et al.* 2005), the proposed method allowed to directly assess  $G''$ . The direct quantitative measurement of the loss modulus is needed to deduce the viscosity parameter in materials presenting low dispersive elasticity as a function of frequency (as in Fig. 6d-e for the mimicking aorta). To our knowledge, vascular ultrasound shear-wave dynamic microelastography has not been reported before in the literature.

In this study, VDME was used to characterize mechanical parameters of vessels in the radial direction. Indeed, because waves induced tissue shearing in the  $y$  direction (see Figs. 5 and 6) and because the IP formulation considered information along lines following the  $x$  axis, the wall artery was mainly excited radially. This information is not available by other techniques that mainly investigate vessels longitudinally or transversely with uniaxial tensile-testing devices, despite the fact that arteries are anisotropic in their cross-sectional plane (Vito *et al.* 2003). Silver *et al.* (2003) used static mechanical tests (*i.e.*, after the stress had relaxed to an equilibrium state) to characterize six porcine abdominal aortic segments. Calculated mean transverse elastic moduli were found to be 19 kPa. Sokolis (2007) used the same protocol on 10 similar vessel segments and estimated an elastic shear modulus of 13 kPa. We found smaller elasticity values radially for the pig artery when one extrapolates data of Figure 6d to a frequency of 0 Hz (static conditions). This could be explained when one considers that smooth muscles, which constitute the media and present a fibrous organization, have a nearly circumferential orientation (Vito *et al.* 2003). This particular microscopic organization confers to the vessel more rigidity in the circumferential direction than in the radial one. Interestingly, as seen in Figure 6d (porcine aortic data), the complex mechanical behavior of such biologic tissue cannot be predicted by simple two-parameter (elasticity  $\mu$ , viscosity  $\eta$ ) Voigt viscoelastic model, defined as  $G(\omega) = \mu + i\omega\eta$ , since  $G'$  strongly increased as a function of frequency. As proposed by Craiem and Armentano (2007), more complex viscoelastic laws describing dynamic behaviors of arterial walls need to be used.

### Selection of the shear wave frequency

The frequency ranges explored using both DME and VDME methods depended mainly on three parameters: the signal-to-noise ratio of the shear wave displacement amplitude maps, the probed material viscoelasticity and the size of the mechanical heterogeneity. For homogeneous tissues, the complex shear modulus was estimated over a wider frequency range for stiffer materials (as seen in Fig. 3) than for softer and more viscous ones (see Fig. 4) since the attenuation was more important in these later. For vascular geometries, it was necessary to have sufficient wavelengths in the artery wall to ensure an accurate estimation of mechanical parameters using the inverse problem strategy. As seen in Figure 6, the very stiff porcine arterial wall had to be characterized at higher frequencies than the mimicked agar-gelatin softer one.

### CONCLUSION

The dynamic micro-elastography technique described in this article could be a suitable tool to explore, in a wide frequency range, the dynamic mechanical properties of soft materials and living tissues, particularly those presenting a microscopic fiber organization. In addition, high spatial resolution shear wave displacement maps (microscopic scale) should be adequate to detect small mechanical heterogeneities. With additional studies to fully validate the method, reported preliminary results suggest the possibility of using VDME for different vascular applications, namely as an *in vitro* tool to characterize viscoelasticity of animal or human vessels, or as an *in vivo* imaging technique (e.g., for monitoring arterial function during medication or during the progression of a disease).

*Acknowledgments*—This research was supported by grants from the Canadian Institutes of Health Research (#MOP-84358) and the Natural Sciences and Engineering Research Council of Canada (#STPGP-381136-09). Cédric Schmitt received a partial Ph.D. scholarship and Dr Anis Hadj Henni a partial post-doctoral fellowship from the Groupe de Recherche en Sciences et Technologies Biomédicales of the Institute of Biomedical Engineering of the University of Montreal.

### REFERENCES

Bercoff J, Tanter M, Fink M. Supersonic shear imaging: A new technique for soft tissue elasticity mapping. *IEEE Trans Ultrason Ferroelectr Freq Control* 2004;51:396–409.

Catheline S, Gennisson JL, Delon G, Fink M, Sinkus R, Abouelkaram S, Culioli J. Measuring of viscoelastic properties of homogeneous soft solid using transient elastography: An inverse problem approach. *J Acoust Soc Am* 2004;116:3734–3741.

Chen S, Urban MW, Pislaru C, Kinnick R, Zheng Y, Yao A, Greenleaf JF. Shearwave dispersion ultrasound vibrometry (SDUV) for measuring tissue elasticity and viscosity. *IEEE Trans Ultrason Ferroelectr Freq Control* 2009;56:55–62.

Cherin E, Williams R, Needles A, Liu G, White C, Brown AS, Zhou YQ, Foster FS. Ultrahigh frame rate retrospective ultrasound microimaging and blood flow visualization in mice *in vivo*. *Ultrasound Med Biol* 2006;32:683–691.

Craiem D, Armentano RL. A fractional derivative model to describe arterial viscoelasticity. *Biorheology* 2007;44:251–263.

Deffieux T, Montaldo G, Tanter M, Fink M. Shear wave spectroscopy for *in vivo* quantification of human soft tissues visco-elasticity. *IEEE Trans Med Imaging* 2009;28:313–322.

Hadj Henni A, Schmitt C, Cloutier G. Analytical modeling of plane shear wave diffraction by a radially layered cylinder for dynamic vascular elastography. *IEEE Ultrason Symp* 2007;1713–1716.

Hadj Henni A, Schmitt C, Cloutier G. 3-D transient and harmonic shear-wave scattering by a soft cylinder for dynamic vascular elastography. *J Acoust Soc Am* 2008;124:2394–2405.

Kruse SA, Rose GH, Glaser KJ, Manduca A, Felmlee JP, Jack CR Jr, Ehman RL. Magnetic resonance elastography of the brain. *Neuroimage* 2008;39:231–237.

Kruse SA, Smith JA, Lawrence AJ, Dresner MA, Manduca A, Greenleaf JF, Ehman RL. Tissue characterization using magnetic resonance elastography: Preliminary results. *Phys Med Biol* 2000;45:1579–1590.

Liao D, Amett DK, Tyroler HA, Riley WA, Chambless LE, Szklo M, Heiss G. Arterial stiffness and the development of hypertension. The ARIC study. *Hypertension* 1999;34:201–206.

Lopez O, Amrami KK, Manduca A, Ehman RL. Characterization of the dynamic shear properties of hyaline cartilage using high-frequency dynamic MR elastography. *Magn Reson Med* 2008;59:356–364.

Muthupillai R, Lomas DJ, Rossman PJ, Greenleaf JF, Manduca A, Ehman RL. Magnetic-resonance elastography by direct visualization of propagating acoustic strain waves. *Science* 1995;269:1854–1857.

Nicolle S, Lounis M, Willinger R, Palierne JF. Shear linear behavior of brain tissue over a large frequency range. *Biorheology* 2005;42:209–223.

Othman SF, Xu H, Royston TJ, Magin RL. Microscopic magnetic resonance elastography (microMRE). *Magn Reson Med* 2005;54:605–615.

Salameh N, Larrat B, Abarca-Quinones J, Pallu S, Dorvillius M, Leclercq I, Fink M, Sinkus R, Van Beers BE. Early detection of steatohepatitis in fatty rat liver by using MR elastography. *Radiology* 2009;253:90–97.

Salameh N, Peeters F, Sinkus R, Abarca-Quinones J, Annet L, Ter Beek LC, Leclercq I, Van Beers BE. Hepatic viscoelastic parameters measured with MR elastography: Correlations with quantitative analysis of liver fibrosis in the rat. *J Magn Reson Imaging* 2007;26:956–962.

Samani A, Zubovits J, Plewes D. Elastic moduli of normal and pathological human breast tissues: An inversion-technique-based investigation of 169 samples. *Phys Med Biol* 2007;52:1565–1576.

Sandrin L, Tanter M, Catheline S, Fink M. Shear modulus imaging with 2-D transient elastography. *IEEE Trans Ultrason Ferroelectr Freq Control* 2002;49:426–435.

Sarvazyan AP, Rudenko OV, Swanson SD, Fowlkes JB, Emelianov SY. Shear wave elasticity imaging: A new ultrasonic technology of medical diagnostics. *Ultrasound Med Biol* 1998;24:1419–1435.

Silver FH, Snowhill PB, Foran DJ. Mechanical behavior of vessel wall: A comparative study of aorta, vena cava, and carotid artery. *Ann Biomed Eng* 2003;31:793–803.

Sokolis DP. Passive mechanical properties and structure of the aorta: Segmental analysis. *Acta Physiol (Oxf)* 2007;190:277–289.

Sunagawa K, Kanai H. Measurement of shear wave propagation and investigation of estimation of shear viscoelasticity for tissue characterization of the arterial wall. *J Med Ultrason* 2005;32:39–47.

Tanter M, Bercoff J, Athanasiou A, Deffieux T, Gennisson JL, Montaldo G, Muller M, Tardivon A, Fink M. Quantitative assessment of breast lesion viscoelasticity: Initial clinical results using supersonic shear imaging. *Ultrasound Med Biol* 2008;34:1373–1386.

Taylor LS, Porter BC, Rubens DJ, Parker KJ. Three-dimensional sonoelastography: Principles and practices. *Phys Med Biol* 2000;45:1477–1494.

Vappou J, Maleke C, Konofagou EE. Quantitative viscoelastic parameters measured by harmonic motion imaging. *Phys Med Biol* 2009;54:3579–3594.

Vito RP, Dixon SA. Blood vessel constitutive models-1995-2002. *Annu Rev Biomed Eng* 2003;5:413–439.

- Wang MH, Palmeri ML, Guy CD, Yang L, Hedlund LW, Diehl AM, Nightingale KR. *In vivo* quantification of liver stiffness in a rat model of hepatic fibrosis with acoustic radiation force. *Ultrasound Med Biol* 2009;35:1709–1721.
- Woodrum DA, Romano AJ, Lerman A, Pandya UH, Brosh D, Rossman PJ, Lerman LO, Ehman RL. Vascular wall elasticity measurement by magnetic resonance imaging. *Magn Reson Med* 2006;56:593–600.
- Yeh WC, Li PC, Jeng YM, Hsu HC, Kuo PL, Li ML, Yang PM, Lee PH. Elastic modulus measurements of human liver and correlation with pathology. *Ultrasound Med Biol* 2002;28:467–474.
- Yin M, Woollard J, Wang X, Torres VE, Harris PC, Ward CJ, Glaser KJ, Manduca A, Ehman RL. Quantitative assessment of hepatic fibrosis in an animal model with magnetic resonance elastography. *Magn Reson Med* 2007;58:346–353.
- Zhang X, Kinnick RR, Fatemi M, Greenleaf JF. Noninvasive method for estimation of complex elastic modulus of arterial vessels. *IEEE Trans Ultrason Ferroelectr Freq Control* 2005;52:642–652.
- Zhou YQ, Foster FS, Qu DW, Zhang M, Harasiewicz KA, Adamson SL. Applications for multifrequency ultrasound biomicroscopy in mice from implantation to adulthood. *Physiol Genomics* 2002;10:113–126.